Spectroscopic signature of strong dielectronic recombination in highly ionized xenon produced by irradiating a gas puff with laser

R. Doron, E. Behar, P. Mandelbaum, and J. L. Schwob
Racah Institute of Physics, The Hebrew University, 91904 Jerusalem, Israel

H. Fiedorowicz, A. Bartnik, R. Jarocki, and M. Szczurek
Institute of Optoelectronics, Military University of Technology, 2 Kaliskiego Street, 01-489 Warsaw, Poland

T. Wilhein
Institute of X-Ray Physics, University of Göttingen, Geiststrasse 11, D-37073 Göttingen, Germany
(Received 25 March 1998; revised manuscript received 28 August 1998)

Highly stripped xenon is produced by irradiating a gas-puff target with a laser pulse of 1-ns duration at an intensity of 10^{13} W/cm^2. The spectrum in the 16.5–19.5-Å wavelength range is measured using a grazing incidence diffractive spectrograph. Spectral lines of Fe-, Co-, Ni-, and Cu-like xenon arising from $3d$-$4p$ radiative transitions are identified. A collisional-radiative model that includes dielectronic capture processes and radiation trapping is used to achieve the line identification and to describe the relative line intensities. The results of the model clearly show that the relatively strong intensities of the $3d^9 4l$-$3d^8 4p 4l$ Ni-like quasicontinuum emission between 17.8 and 18.4 Å arise from dielectronic recombination processes, which probably take place during the cooling phase of the plasma. The resonant nature of the dielectronic recombination processes enables us to diagnose the average electron temperature of the plasma during the recombination phase, and it is found to be about 150 eV. [S1050-2947(99)01101-4]

PACS number(s): 32.30.Rj, 32.70.−n, 52.70.−m

I. INTRODUCTION

It has already been demonstrated that a hot and dense plasma can be produced by irradiating a gas-puff target with a nanosecond high-power laser pulse [1,2]. Plasmas produced in gas-puff targets have the advantage of being debris-less x-ray sources, which makes them suitable for x-ray lithography and microscopy applications. Also, gas target plasmas have relatively small density gradients compared to solid target plasmas, which is important for creating x-ray lasing conditions. In Ref. [3] a soft-x-ray spectrum in the 80–120-Å wavelength range emitted from a laser-produced xenon plasma was obtained, and lasing was demonstrated. The laser-produced Xe plasma is of particular interest since the conversion efficiency of laser energy into x-ray energy in Xe was shown to be relatively high (5.4%), comparable to the efficiency in solid iron and tellurium [4]. Indeed, Xe in ionization states around Ni I emits strong x rays in the vicinity of 14 and 18 Å, corresponding to $3d$-$4f$ and $3d$-$4p$ radiative transitions, respectively. A Xe spectrum in the 13–22-Å wavelength range emitted from the French TFR (Tokamak Fontenay-aux Roses) tokamak was published in the past [5], but that spectrum is significantly different from the present one, and among other differences does not show any spectral lines directly originating from dielectronic recombination (DR).

In contrast to tokamak plasmas, several solid-target laser-produced-plasma experiments for low-Z elements in the Li I to Na I isoelectronic sequences have shown spectroscopic traces of DR originated line emission (e.g., Ref. [6]). However, to the best of our knowledge, there have been almost no such investigations on heavy ions isoelectronic to sequences around Ni I, except for a work on tantalum [7], and a recent work on barium [8]. The experiment described in Ref. [7] was not modeled level by level, and the importance of DR was not assessed quantitatively. In Ref. [8] a two-step level-by-level collisional-radiative model, including dielectronic capture and autoionization processes, was developed for interpreting the experimental x-ray spectrum emitted by a laser-irradiated solid BaF_2 target. In the present work, the soft-x-ray spectrum emitted from a Xe gas-puff target irradiated by a powerful laser is investigated. The spectral features are identified, and the line intensities are analyzed by employing the collisional-radiative model described in Ref. [8], which is extended here to include radiation trapping.

II. EXPERIMENTAL SETUP

The experiment was performed at the Institute of Optoelectronics in Warsaw, Poland. The gas-puff target is created by pulsed injection of small amounts of Xe gas from a high-pressure (10 atm) solenoid valve through a nozzle into a vacuum chamber. A Nd:glass laser of wavelength 1.06 μm with a pulse energy of about 5 J and a pulse duration of 1 ns is focused with an aspherical lens of 10-cm focal length to a spot with a diameter of approximately 150 μm. The laser beam irradiates the gas perpendicularly to the direction of the gas flow about 200 μm away from the nozzle. The time delay between the opening of the valve and the laser pulse is set to be 0.3 ms to give maximum gas density in the whole laser interaction region. The density of the Xe gas puff is measured using the x-ray backlighting method to be around the maximal density of 10 mg/cc. Although the valve could be used at a repetition rate of 10 Hz, the present experiment is carried out in a single laser shot mode.

The soft-x-ray radiation emitted by the plasma is measured using a calibrated compact spectrograph developed at

the University of Göttingen [9]. The radiation is dispersed by a Ni-covered flat glass-substrate *off-axis reflection zone plate* (ORZ) [10] and is focused onto a soft-x-ray-sensitive charge-coupled-device (CCD) detector. The recorded spectrum is calibrated to account for the wavelength dependence of both the reflection efficiency of the ORZ element and the quantum efficiency of the CCD array. The absorption of an Al filter used to suppress infrared, visible, and UV radiation is also taken into account. The instrumental line broadening of the spectrograph in the wavelength region investigated in this work is about 50 mÅ. A detailed description of the spectrograph, including the calibration procedures, can be found elsewhere [9,11].

III. THEORETICAL METHOD

In a previous work [8], a two-step collisional-radiative (CR) model was developed for simulating the spectra emitted from autoionizing levels. Here this model is employed to describe the level populations and the spectral line intensities of the Fe-, Co-, Ni-, and Cu-like Xe ions. Each pair of adjacent ionization states (Fe I and Co I, or Co I and Ni I, or Ni I and Cu I) is considered in the model at once. For the doubly (or inner-shell) excited levels, the following atomic processes are included: radiative decays and collisional transitions between the doubly excited levels, radiative decays to singly excited levels, excitation and deexcitation from and to singly excited levels, autoionization, dielectronic capture, collisional ionization, and three-body recombination. All the significant configurations have been included in the model: $3d^8$ and $3d^7 4l$ for the Fe-like Xe ion, $3d^9$ and $3d^8 nl$ ($n=4$ and 5) for the Co-like ion, $3d^{10}$, $3d^9 nl$ ($n=4$ and 5), $3d^8 4l 4l'$ (excluding $3d^8 4d 4f$ and $3d^8 4f^2$), and $3d^8 4p 5l'$ for the Ni-like ion, and $3d^{10} 4l$ and $3d^9 4l 4l'$ for the Cu-like ion. All these add up to 531, 508, 3492, and 692 levels for the Fe-, Co-, Ni, and Cu-like Xe ions, respectively. The density ratio of adjacent ionization states, which is a parameter in the model, is deduced from the measured intensity ratio of the strong resonant lines of the two ionization states. For instance, the $n_{\mathrm{Co\ I}}/n_{\mathrm{Ni\ I}}$ ratio is found here to be approximately 0.3. Since the spectrum is time integrated and the time evolution of the plasma is not well known, a steady-state model is used. More information about the detailed procedure carried out in the model can be found in Ref. [8].

In the present work, radiation trapping effects have been included in the collisional-radiative rate equations by correcting the Einstein coefficients using the *mean escape factor* ε_{ij} *approximation*, developed by Breton and Schwob [12]. In this approximation the line intensities I_{ji} are given by introducing a *mean transmission factor* T_{ij}:

$$I_{ji} \propto n_j A_{ji} T_{ij}, \tag{1}$$

where n_j is the number density of ions in level j obtained from the model and A_{ji} is the Einstein coefficient for radiative decay from level j to level i. T_{ij} is found by averaging the photon transmission probability over the whole frequency profile of the spectral line and by integrating along the line of sight in the plasma [12]:

$$T_{ij} = \frac{1}{\tau_{ij}\sqrt{\pi}} \int_{-\infty}^{\infty} \{1 - \exp[-\tau_{ij} \exp(-y^2)]\} dy. \tag{2}$$

Here y is a reduced frequency defined by

$$y = 2 \frac{\nu - \nu_0}{\Delta \nu_D(T_i)} \sqrt{\ln 2} \tag{3}$$

and τ_{ij} is the optical depth of the plasma for the transition $j \rightarrow i$ at the central spectral line frequency ν_0, defined by

$$\tau_{ij} = \frac{2\sqrt{\pi \ln 2}}{\Delta \nu_D(T_i)} \frac{e^2}{m_e c} n_i f_{ij} L. \tag{4}$$

$\Delta \nu_D(T_i)$ is the Doppler width of the line at the ion temperature T_i taken in this work to be equal to the electron temperature T_e. n_i is the number density of ions in the absorbing state i, f_{ij} is the absorption oscillator strength for the transition, and L is the dimension of the plasma along the line of sight taken here to be about 150 μm. It has been shown [12] for a cylindric plasma that the mean escape factor ε_{ij} for the whole plasma, which is a obtained by integration in all directions, is very close to the mean transmission factor T_{ij} along a transversal direction through the center of the plasma. Therefore, ε_{ij} can be replaced by T_{ij} in the rate equations to make calculations easier. The number density n_i of the absorbing level i [Eq. (4)] is computed self-consistently by solving the CR rate-equation system through successive iterations. It should be noted that for the transitions involving the doubly excited levels, the radiation trapping effects are negligible at the ion density considered in the present experiment. Therefore, in order to save considerable computing time, the transmission coefficients are introduced in the rate equations in the first step of the model only for transitions involving the ground and the singly excited levels. The atomic quantities (energy levels, autoionization coefficients, radiative and collisional rate coefficients) needed for the model are calculated using the multiconfiguration relativistic HULLAC (Hebrew University Lawrence Livermore Atomic Code) computer package [13].

IV. RESULTS AND DISCUSSION

A. Comparison between theoretical and experimental spectra

The experimental Xe spectrum in the 16.5–19.5-Å wavelength range is shown in Fig. 1 (thick trace). Below it, the synthetic spectrum calculated by using the CR model (with the electron temperature and density as discussed later in Sec. IV C) is presented (thin trace). The theoretical lines are given a uniform Gaussian profile which is chosen to be slightly narrower than the narrowest experimental line widths (≈50-mÅ full width at half maximum). The relative line intensities emitted *within* each ionization state are directly obtained from the model, whereas the intensity ratios of lines from different ionization states are set to fit the experimental spectrum. In order to clearly show the contributions of each of the Fe-, Co-, Ni-, and Cu-like ionization states to the spectrum, the partial theoretical spectrum calculated for each ion species separately (with an arbitrary very small linewidth) is given in Fig. 1 below the synthetic spec-

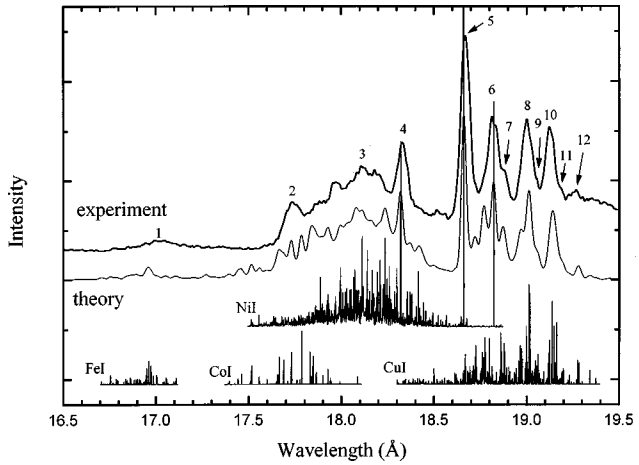

FIG. 1. Experimental spectrum of $3d$-$4p$ transitions in highly ionized Xe in the 16.5–19.5-Å wavelength range compared to the theoretical spectrum. Labels correspond to the transition identifications in Table I. The four plots below the full trace give the calculated partial spectrum of each Xe ionization state separately (with an arbitrary very narrow linewidth).

trum trace. It can be seen from the partial plots in Fig. 1 that the Ni- and Cu-like Xe ions give the dominant x-ray emission, while there is only one observable Co-like peak in the experimental spectrum and one very weak Fe-like feature. Also, in most places the model predicts no overlap between strong lines of different ionization states. It is important to note that calculations of line wavelengths alone give thousands of Co-, Ni-, and Cu-like Xe lines arising from $3d$-$4p$ transitions with different electron spectators in the wavelength region given in Fig. 1. Hence, in order to identify the 11 resolved peaks observed in the experimental spectrum, and in order to interpret the quasicontinuum structure denoted in Fig. 1 by the label 3, a straightforward comparison between computed and measured line wavelengths is insufficient. Therefore, it is also necessary to model the line intensities using the CR model described above. It is found that self-absorption effects [Eqs. (1)–(4)] must also be taken into account to explain the relatively low intensities of the Ni-like $3d^{10}$-$3d^9 4p$ resonant lines, especially the peak labeled 5 in Fig. 1. For all the other lines, originating from doubly excited levels, self-absorption was also calculated, but is found to be almost negligible.

The comparison between the experimental and theoretical spectra allows the identification of all the observed peaks labeled in Fig. 1. The line identifications are presented in Table I. The line labels are given in the first column. The second column shows the line wavelengths in Ångströms λ_{exp}(Å) as measured in the present work. Where available, the wavelengths previously measured in Ref. [5] are given for comparison. Actually, the wavelengths of lines 4 and 5 were taken from the low-density plasma spectrum in Ref. [5] and used here for the wavelength calibration. The wavelength of the Co-like peak (labeled 2) could not have been measured correctly in Ref. [5], due to blending with an oxygen line in the tokamak spectrum. The fourth column gives the ionization state and the isoelectronic sequence of the emitting Xe ion. The theoretical wavelengths λ_{th}(Å) calculated here are given in the next column, followed by the calculated Einstein coefficient for spontaneous emission A_{ji} of the transition considered. The next column displays the identified radiative transition. For the upper level of the transition, only the most important components of the eigenvector are given, preceded by the square of their coefficients. The last two columns show the total angular momentum of the lower (J_L) and upper (J_U) levels of the transition.

The wide quasicontinuum feature labeled as 3 which appears in the 17.8–18.4-Å range of the spectrum is identified to essentially be the superposition of many coalesced $3d^9 4l$-$3d^8 4p4l$ lines and some weak $3d^9 5l$-$3d^8 4p5l$ lines. In fact, except for the three resonant $3d^{10}$-$3d^9 4p$ lines (labeled 4, 5, and 6) all the Ni-like lines which are plotted in the theoretical narrow-line Ni I spectrum at the bottom of Fig. 1 are $3d^9 nl$-$3d^8 4pnl$ ($n=4$ and 5) lines. The emission from high $3d^8 4pnl (n>5)$ configurations has also been calculated and found to be much weaker than that from $3d^8 4p5l$, which in turn is already much weaker than that of $3d^8 4p4l$. There are many differences between the present Xe laser-produced plasma spectrum and the Xe spectrum from the low-density and much hotter plasma in the TFR tokamak [5]. For example, as expected, the Ni-like $3d$-$4s$ electric quadrupole lines observed in the tokamak spectrum do not appear in the present spectrum. Also, lines from higher ionization states such as Mn- and Cr-like states are observed only in the tokamak plasma. However, most interesting for the present work is the fact that the strong $3d^9 4l$-$3d^8 4p4l$ quasicontinuum feature (label 3) described above is completely absent in the tokamak spectrum.

B. $3d^8 4p4l$ populating processes

There are two main mechanisms by which the Ni-like doubly excited $3d^8 4p4l$ levels can be populated: Inner-shell excitation (ISE) from the singly excited $3d^9 4l$ Ni-like levels, or dielectronic capture (DC) from the Co-like ground states. Three-body recombination is included in the calculations as well, but is found to be still negligible at the present moderate electron density. Since the $3d^8 4p4l$ levels are not directly accessible from the Ni-like ground state, the excitation mechanism from the ground state is possible only by at least two consecutive excitations. The two-step mechanism can be schematically described as:

$$3d^{10} + e^- \rightarrow 3d^9 4l + e^- \tag{5}$$

followed by inner-shell excitation

$$3d^9 4l + e^- \rightarrow 3d^8 4p4l + e^-. \tag{5'}$$

The DC mechanism can be schematically represented as:

$$3d^9 + e^- \rightarrow 3d^8 4p4l. \tag{6}$$

Both the inner-shell excitation and the dielectronic capture can be followed by a radiative decay through a $3d$-$4p$ transition,

$$3d^8 4p4l \rightarrow 3d^9 4l + h\nu, \tag{7}$$

with the emission of a soft-x-ray photon ($h\nu$). Since this emission is the same whether originating from ISE or from DC, a more detailed analysis is needed in order to determine the relative importance of each mechanism.

TABLE I. Experimental and theoretical line wavelengths in the 16.9–19.3-Å range and the corresponding $3d$-$4p$ transitions identified in Fe-, Co-, Ni-, and Cu-like Xe ions. Labels refer to the peaks of the experimental spectrum in Fig. 1. Only theoretical wavelengths of the strongest lines are given. A few wavelengths measured in the TFR tokamak (Ref. [5]) are also given. A_{ji} represents the Einstein coefficient for spontaneous emission: $X(Y)$ stands for $X\times10^{Y}$. For the upper level of the transitions the most important component of the eigenvector is given, preceded by the square of its coefficient. J_L and J_U are the total angular momenta of the lower and upper levels, respectively.

Label	λ_{expt} (Å)	λ_{expt} (Å) Ref. [5]	Ion (sequence)	λ_{th} (Å)	A_{ji} (s^{-1})	Line transition or unresolved transition array	J_L	J_U
1	16.9–17.1	17.0	Xe^{28+} (Fe I)	16.960		$3d^8$ - $3d^7\,4p$		
2	17.735	17.8	Xe^{27+} (Co I)	17.665	9.4(11)	$3d^9$ - 76%$(3d^3_{3/2}3d^5_{5/2})_4 4p_{3/2}$	$\frac{3}{2}$	$\frac{5}{2}$
			Xe^{27+} (Co I)	17.688	1.4(12)	$3d^9$ - 73%$(3d^4_{3/2}3d^4_{5/2})_2 4p_{3/2}$	$\frac{5}{2}$	$\frac{3}{2}$
			Xe^{27+} (Co I)	17.729	1.2(12)	$3d^9$ - 75%$(3d^3_{3/2}3d^5_{5/2})_2 4p_{3/2}$	$\frac{3}{2}$	$\frac{3}{2}$
			Xe^{27+} (Co I)	17.731	1.1(12)	$3d^9$ - 91%$(3d^4_{3/2}3d^4_{5/2})_2 4p_{3/2}$	$\frac{5}{2}$	$\frac{5}{2}$
			Xe^{27+} (Co I)	17.786	1.4(12)	$3d^9$ - 71%$(3d^3_{3/2}3d^5_{5/2})_4 4p_{1/2}$	$\frac{5}{2}$	$\frac{7}{2}$
3	17.8–18.4		Xe^{26+} (Ni I)	17.8–18.4		$3d^9 4l$ - $3d^8 4l 4p$		
4	18.326	18.326	Xe^{26+} (Ni I)	18.322	3.0(11)	$3d^{10}$ - 96% $3d^9_{3/2}4p_{3/2}$	0	1
5	18.667	18.667	Xe^{26+} (Ni I)	18.661	2.0(12)	$3d^{10}$ - 88% $3d^9_{5/2}4p_{3/2}$	0	1
6	18.826	18.826	Xe^{26+} (Ni I)	18.822	3.9(11)	$3d^{10}$ - 90% $3d^9_{3/2}4p_{1/2}$	0	1
7	18.870		Xe^{25+} (Cu I)	18.860	5.0(11)	$3d^{10}4s$ - 60% $(3d^9_{5/2}4s)_3 4p_{3/2}$	$\frac{1}{2}$	$\frac{3}{2}$
			Xe^{25+} (Cu I)	18.866	3.6(11)	$3d^{10}4d$ - 32%$(3d^9_{5/2}4p_{3/2})_1 4d_{5/2}$	$\frac{5}{2}$	$\frac{7}{2}$
						$+23\%(3d^9_{5/2}4p_{3/2})_4 4d_{5/2}$		
			Xe^{25+} (Cu I)	18.879	8.8(11)	$3d^{10}4d$ - 40%$(3d^9_{5/2}4p_{3/2})_1 4d_{5/2}$	$\frac{5}{2}$	$\frac{5}{2}$
						$+16\%(3d^9_{5/2}4p_{3/2})_3 4d_{5/2}$		
8	19.000		Xe^{25+} (Cu I)	18.998	1.4(12)	$3d^{10}4p$ - 81% $3d^9_{5/2}(4p^2_{3/2})_2$	$\frac{3}{2}$	$\frac{3}{2}$
			Xe^{25+} (Cu I)	19.012	1.5(12)	$3d^{10}4p$ - 81% $3d^9_{5/2}(4p^2_{3/2})_2$	$\frac{3}{2}$	$\frac{5}{2}$
			Xe^{25+} (Cu I)	19.018	1.9(12)	$3d^{10}4p$ - 71%$(3d^9_{5/2}4p_{1/2})_3 4p_{3/2}$	$\frac{1}{2}$	$\frac{3}{2}$
9	19.055		Xe^{25+} (Cu I)	19.048	3.1(11)	$3d^{10}4d$ - 35%$(3d^9_{5/2}4p_{3/2})_4 4d_{5/2}$	$\frac{5}{2}$	$\frac{7}{2}$
						$+21\%(3d^9_{5/2}4p_{3/2})_4 4d_{3/2}$		
			Xe^{25+} (Cu I)	19.062	1.1(12)	$3d^{10}4p$ - 89%$(3d^9_{5/2}4p_{1/2})_2 4p_{3/2}$	$\frac{1}{2}$	$\frac{1}{2}$
10	19.124		Xe^{25+} (Cu I)	19.138	6.4(11)	$3d^{10}4f$ - 62%$(3d^9_{3/2}4p_{1/2})_1 4f_{7/2}$	$\frac{7}{2}$	$\frac{9}{2}$
			Xe^{25+} (Cu I)	19.138	6.2(11)	$3d^{10}4d$ - 39%$(3d^9_{3/2}4p_{1/2})_1 4d_{5/2}$	$\frac{5}{2}$	$\frac{7}{2}$
						$+15\%(3d^9_{5/2}4p_{3/2})_2 4d_{3/2}$		
			Xe^{25+} (Cu I)	19.139	6.2(11)	$3d^{10}4d$ - 51%$(3d^9_{3/2}4p_{1/2})_1 4d_{5/2}$	$\frac{5}{2}$	$\frac{5}{2}$
			Xe^{25+} (Cu I)	19.148	1.9(12)	$3d^{10}4s$ - 76% $(3d^9_{5/2}4s)_2 4p_{3/2}$	$\frac{1}{2}$	$\frac{1}{2}$
			Xe^{25+} (Cu I)	19.163	9.1(11)	$3d^{10}4s$ - 75% $(3d^9_{5/2}4s)_2 4p_{3/2}$	$\frac{1}{2}$	$\frac{3}{2}$
11	19.185		Xe^{25+} (Cu I)	19.195	5.3(11)	$3d^{10}4p$ - 80%$(3d^9_{3/2}4p_{1/2})_1 4p_{3/2}$	$\frac{3}{2}$	$\frac{1}{2}$
			Xe^{25+} (Cu I)	19.199	1.6(11)	$3d^{10}4p$ - 65%$(3d^9_{3/2}4p_{1/2})_2 4p_{3/2}$	$\frac{3}{2}$	$\frac{5}{2}$
12	19.268		Xe^{25+} (Cu I)	19.277	3.2(11)	$3d^{10}4s$ - 62% $(3d^9_{3/2}4s)_2 4p_{1/2}$	$\frac{1}{2}$	$\frac{3}{2}$
			Xe^{25+} (Cu I)	19.285	3.5(11)	$3d^{10}4d$ - 53%$(3d^9_{3/2}4p_{1/2})_2 4d_{3/2}$	$\frac{3}{2}$	$\frac{5}{2}$

The contribution of each of these two main mechanisms responsible for populating the $3d^8 4p 4l$ levels has been thoroughly investigated here. Figure 2 shows the theoretical spectra for three different electron temperatures: $kT_e=100$, 140, and 250 eV (at $n_e=10^{21}$ cm^{-3} and $n_{\mathrm{Co\,I}}/n_{\mathrm{Ni\,I}}=0.3$) in the spectrum portion comprising the $3d$-$4p$ Ni-like Xe emission. The temperature of 140 eV seems to give the best fit between theoretical and experimental spectra. For each temperature, the contribution of the DC processes (dashed curves) and that of the ISE processes (dotted curves) are given separately for comparison. It can be seen that at 100 eV [Fig. 2(A)] and at 140 eV [Fig. 2(B)] the $3d^9 4l$-$3d^8 4p 4l$ transitions originate predominantly from DC processes, while the contribution of the ISE processes is very small. At 250 eV [Fig. 2(C)], the emission of the $3d^9 4l$-$3d^8 4p 4l$ transitions is relatively weak, but still one can notice that, contrary to the low-temperature cases, the ISE processes dominate over the DC processes.

In order to extend the analysis of Fig. 2 to temperatures beyond 250 eV, and in order to more accurately define the electron temperature range in which the DC mechanism dominates, in Fig. 3 we have plotted the ratio of the calculated populating rate for the doubly excited levels by DC to that by ISE in the wide temperature range $100\ \mathrm{eV}\leqslant kT_e\leqslant 1000$ eV. These calculations are performed assuming the present plasma conditions, i.e., $n_e=10^{21}$ cm^{-3} and $n_{\mathrm{Co\,I}}/n_{\mathrm{Ni\,I}}=0.3$, and the absorption parameters indicated in Sec. III. It can be seen that, for temperatures lower than 200 eV, DC is the dominant populating mechanism, whereas for temperatures above 250 eV ISE dominates. In Sec. IV C we will show, however, that this dominance of ISE at high temperatures does not give rise to a strong quasicontinuum emission (label 3) with respect to the resonant lines [see Fig. 2(C)], and therefore cannot explain the present experimental results.

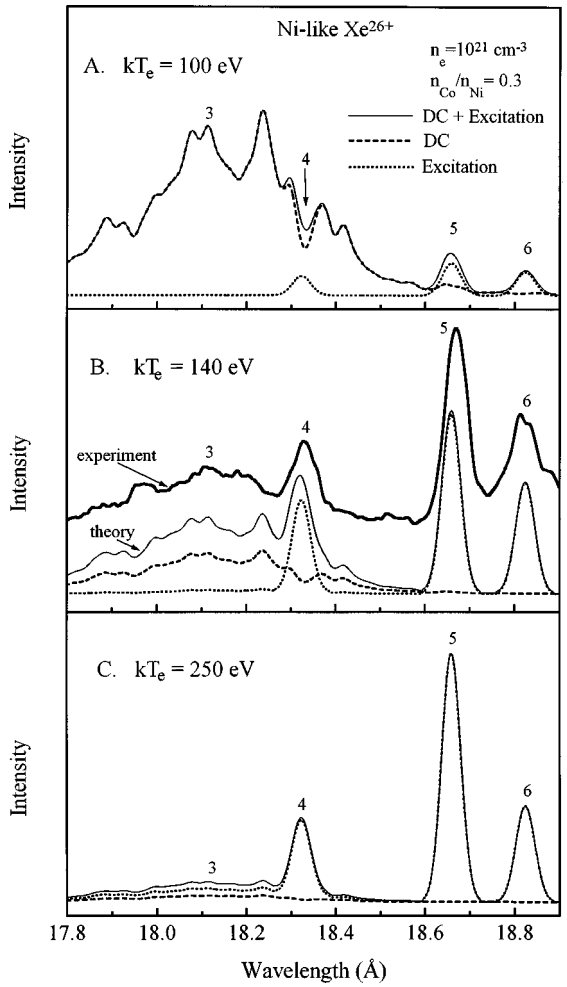

FIG. 2. Theoretical spectra (thin solid curves) of the $3d$-$4p$ Ni-like Xe transitions for three different electron temperatures: 100 eV (A), 140 eV (B), and 250 eV (C) calculated at $n_e = 10^{21}$ cm^{-3} and $n_{\mathrm{Co\,I}}/n_{\mathrm{Ni\,I}} = 0.3$. The dashed and dotted curves indicate the spectral components originating from dielectronic capture (DC) only and from collisional excitation only, respectively. The thick trace in (B) is the experimental spectrum. Labels correspond to the transition identifications in Table I.

C. Electron temperature estimate

The electron density in the present experiment is assumed to be 10^{21} cm^{-3}. This density, which is just about the critical density of the plasma for still absorbing the 1.06-μm laser radiation, has been directly measured in a similar previous experiment with an argon gas-puff target [14]. The density ratios of adjacent ionization states (e.g., $n_{\mathrm{Co\,I}}/n_{\mathrm{Ni\,I}}$) are deduced from the experimental spectrum as mentioned in Sec. III. Hence the sole remaining free parameter of the model is the electron temperature. It is found that most of the spectral features within each ionization state can be reproduced by the model with an electron temperature of about 250 eV (this is the temperature introduced for calculating the spectrum in Fig. 1, except for the feature 3). However, the quasicontinuum emission arising from the $3d^9 4l$-$3d^8 4p4l$ Ni-like transitions (labeled 3) cannot be adequately reproduced at such a high temperature, indicating that these lines arise from dielectronic captures which occur at temperatures much lower than 250 eV.

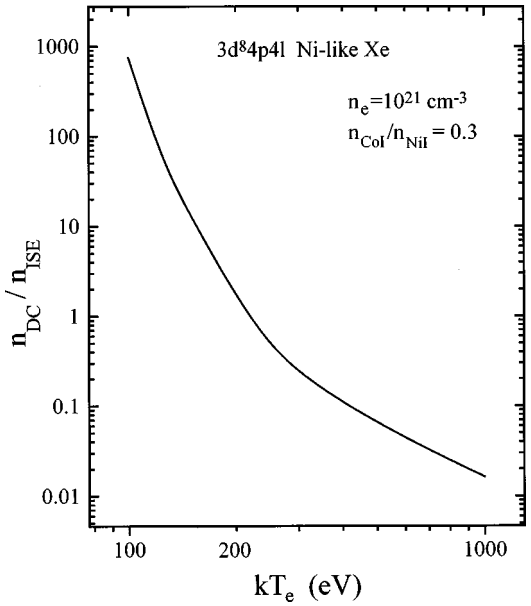

FIG. 3. Calculated ratio of the DC populating contribution (n_{DC}) to the ISE populating contribution (n_{ISE}) for the $3d^8 4p4l$ levels as a function of the electron temperature.

The fact that a low electron temperature, of the order of 150 eV or less, can account for the strong $3d^9 4l$-$3d^8 4p4l$ quasicontinuum emission (labeled 3) observed in the experiment has already been shown in Fig. 2(B). At these temperatures the quasicontinuum emission is significantly strong and almost comparable to the intensity of the resonant $3d^{10}$-$3d^9 4p$ lines (labeled 4, 5, and 6). In order to show that this effect cannot also occur at very high temperatures as a result of the ISE processes, synthetic spectra have been calculated for both the quasicontinuum $3d^9 4l$-$3d^8 4p4l$ emission and the resonant $3d^{10}$-$3d^9 4p$ lines in a wide range of temperatures. The intensity ratios of the quasicontinuum peak (labeled 3) to the resonant line peaks (labeled 5 and 6) as a function of the temperature are shown in Fig. 4. Line intensity calculations have also been carried out for peak 4, giving ratios which are very similar to those for peak 6. The high intensity ratios observed in Fig. 4 at low electron temperatures are attributed to the steep rise of the DC rates as T_e decreases. At high electron temperatures the dominant population mechanism is collisional excitation. However, at these temperatures the collisional excitation processes enhance the populations of both the singly and the doubly excited levels. In addition, the resonant lines are less attenuated by self-absorption at high temperatures due to the higher ion temperatures and due to the relatively lower population of the absorbing ground state. Therefore, only a moderate increase of the intensity ratio is observed at very high temperatures (Fig. 4). It is clear from the figure that even at $kT_e = 1000$ eV the line intensity ratios do not reach the relatively high experimental values indicated in the figure by the horizontal bars. The experimental values rather indicate a low electron temperature of about 150 eV which corresponds to the recombining plasma phase. It should be stressed, however, that the radiation emitted from the hot plasma at early times of the laser interaction contributes to the observed intensities of the lines 4, 5, and 6, as well, and therefore $kT_e \cong 150$ eV is actually the temporally averaged temperature of

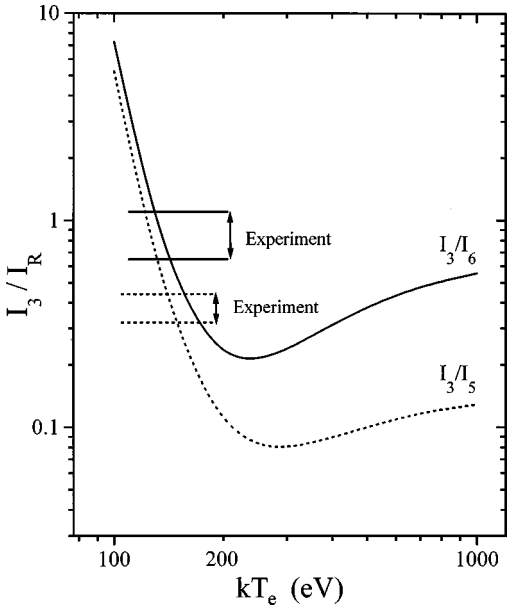

FIG. 4. Calculated intensity ratio of the quasicontinuum peak (I_3) to the peaks of the resonant lines (I_5 and I_6) of the $3d$-$4p$ Ni-like Xe emission as a function of the electron temperature. The experimental ratios are indicated by the horizontal bars, which show the experimental error range.

the plasma. The temperature during the recombination phase is, thus, somewhat lower than 150 eV. It can be seen from Fig. 4 that the experimental I_3/I_5 ratio indicates a slightly higher average temperature than the I_3/I_6 ratio. This can be explained by the fact that as the temperature of the plasma decreases, absorption increases, and line 5 (which is particularly highly absorbed at low temperatures due to its high oscillator strength value) is more attenuated than line 6 (and 4). The difference in average temperature indication is, thus, a result of the early emission from the hot plasma having a larger influence on the time integrated intensity of line 5.

One notices in the experimental spectrum that the Ni-like transition array originating from DC is even slightly more intense than the Co-like resonant lines. This can be explained by the fact that the observed spectrum mostly reflects the relatively low-temperature recombination phase. At this low-temperature collisional excitation from the Co-like ground levels becomes less important than the DC mechanism from those levels. In addition, the Co-like resonant lines are attenuated by self absorption.

At electron temperatures lower than 150 eV, the Ni-like $3d^9 4l$-$3d^8 4p4l$ quasicontinuum emission can become even more intense than the Ni-like $3d^{10}$-$3d^9 4p$ transitions [as can be seen in Fig. 2(A)]. Thus in this temperature range the theoretical spectrum could be fitted to the experimental one by significantly decreasing the value of the $n_{\mathrm{Co\ I}}/n_{\mathrm{Ni\ I}}$ parameter in the model. For instance, at $kT_e = 100$ eV, the required value for the $n_{\mathrm{Co\ I}}/n_{\mathrm{Ni\ I}}$ ratio is about 0.04. However such a low value should be ruled out since it is in total disagreement with the ratio experimentally deduced from other emission features in the spectrum, which indicates a value of about 0.3. On the other hand, at higher temperatures ($kT_e \geqslant 250$ eV) the theoretical intensity ratios of the lines originating from doubly excited levels to those originating from singly excited levels are independent of the $n_{\mathrm{Co\ I}}/n_{\mathrm{Ni\ I}}$ parameter, since the spectrum almost purely originates form collisional excitations.

One may ask why the analogous DR processes for the neighboring Cu- or Zn-like ionization states do not give rise to strong broad spectral features as for the Ni-like ions. The reason is that almost all the Cu-like $3d^9 4p4l$ levels lie below the ionization limit (and thus cannot be directly populated by DC), except for the $3d^9 4p4f$ configuration. But, the $3d^9 4p4f$ levels have a much stronger tendency for $3d$-$4f$ radiative decays than for $3d$-$4p$ radiative transitions, which could be observed in the present recorded spectral range. The same explanation holds for the Zn-like $3d^9 4s4p4l$ configurations.

V. CONCLUSIONS

To summarize, the present collisional-radiative model allows the identification of the spectral lines emitted by highly ionized Xe produced by irradiating a gas puff with a powerful laser. The spectrum is quite different from the Xe spectrum measured from the TFR tokamak. The remarkable spectral feature observed in the present experiment is the strong quasicontinuum emission between 17.8 and 18.4 Å, which is identified as originating from $3d^9 4l$-$3d^8 4p4l$ radiative decays. The strong $3d^9 4l$-$3d^8 4p4l$ emission is interpreted as a clear signature of dielectronic captures which take place during the cooling phase of the recombining plasma.

ACKNOWLEDGMENTS

One of the authors (E.B.) was supported by the Charles Clore Israel Foundation. The experimental work at the Institute of Optoelectronics in the Military University of Technology in Warsaw was partially supported by the State Committee for Scientific Research of Poland under Grant No. 2 P03B 013 11 and by the German Federal Ministry of Education and Research (BMBF) under Contract No. 13N6491.

[1] H. Fiedorowicz, A. Bartnik, Z. Patron, and P. Parys, Appl. Phys. Lett. **62**, 2778 (1993).

[2] H. Fiedorowicz, A. Bartnik, Z. Patron, and P. Parys, Laser Part. Beams **12**, 471 (1994).

[3] H. Fiedorowicz, A. Bartnik, Y. Li, P. Lu, and E. Fill, Phys. Rev. Lett. **76**, 415 (1996).

[4] H. Fiedorowicz, A. Bartnik, J. Kostecki, and M. Szczurek, *E-Beam, X-Ray, EUV, and Ion-Beam Lithographies*, edited by D. E. Seeger, Proceedings of SPIE Vol. 2723 (SPIE, Bellingham, WA, 1996).

[5] J. F. Wyart, C. Bauche-Arnoult, E. Luc-Koenig, and TFR Group, Phys. Scr. **32**, 103 (1985).

[6] J. Nilsen, U. I. Safranova, S. Safranova, and L. A. Vainshtein, Phys. Scr. **51**, 589 (1995).

[7] C. Bauche-Arnoult, J. Bauche, E. Luc-Koenig, J. F. Wyart, R. M. More, C. Chenais-Popovics, J. C. Gauthier, J. P. Geindre, and N. Tragin, Phys. Rev. A **39**, 1053 (1989).

[8] R. Doron, E. Behar, M. Fraenkel, P. Mandelbaum, A. Zigler, J. L. Schwob, A. Ya Faenov, and T. A. Pikuz, Phys. Rev. A **58**, 1859 (1998).

[9] T. Wilhein, D. Hambach, B. Niemann, M. Berglund, L. Rymell, and H. M. Hertz, Appl. Phys. Lett. **71**, 190 (1997).

[10] B. Niemann, T. Wilhein, T. Schliebe, R. Plontke, O. Fortagne, I. Stolberg, and M. Zierbock, Microelectron. Eng. **30**, 49 (1996).

[11] T. Wilhein, D. Altenbernd, U. Teubner, E. Foerster, R. Haessner, W. Theobald, and R. Sauerbrey, J. Opt. Soc. Am. B **15**, 1235 (1998).

[12] C. Breton and J. L. Schwob, C. R. Acad. Sci. Paris **260**, 461 (1965); **261**, 1476 (1965); and in *Some Aspects of VUV Radiation Physics*, edited by N. Damany, B. Vodar, and J. Romand (Pergamon, Oxford, 1974), pp. 250–256.

[13] A. Bar-Shalom, M. Klapisch, and W. H. Goldstein (unpublished).

[14] I. Yu Skobelev, A. Ya Faenov, V. M. Dyakin, H. Fiedorowicz, A. Bartnik, M. Szczurek, P. Beiersdorfer, J. Nilsen, and A. L. Osterheld, Phys. Rev. E **55**, 3773 (1997).